Proceedings World Geothermal Congress 2015
Melbourne, Australia, 19-25 April 2015

Application of Various Geophysical Techniques to Reservoir Monitoring and Modeling

Tsuneo Ishido[1], John W. Pritchett[2], Yuji Nishi[1], Mituhiko Sugihara[1], Sabodh K. Garg[2], Jeffry L. Stevens[2], Toshiyuki Tosha[3], Shigetaka Nakanishi[4] and Shinsuke Nakao[1]

[1] Geological Survey of Japan, National Institute of Advanced Industrial Science and Technology, Tsukuba, 305-8567 Japan; [2]Leidos, Inc., 10260 Campus Point Drive, San Diego, CA 92121, USA; [3]JOGMEC, Tokyo, Japan; [4]J-Power, Tokyo, Japan

Ishido-t@aist.go.jp

Keywords: reservoir monitoring, history-matching, microgravity, self-potential, resistivity, seismic, surface-deformation

ABSTRACT

We have been developing so-called "geophysical postprocessors" since the early 1990's. These computational tools calculate temporal changes in geophysical observables that result from changing underground conditions computed by reservoir simulations. The purpose of the development is to enable us to use monitoring data from repeat and/or continuous geophysical measurements in history-matching studies. We first developed a microgravity postprocessor, and then developed postprocessors for self-potential, electrical resistivity (DC or MT), magnetic, seismic (reflection, VSP or cross-hole) and surface-deformation measurements so far under various geothermal and CCS projects in Japan. Among recent topics, we present the results of history-matching studies using self-potential and gravity data, and introduce recent improvements made in the self-potential, seismic and surface-deformation postprocessors.

1. INTRODUCTION

Numerical models of geothermal reservoirs are never precise, owing to the problem of non-uniqueness. The difficulty increases as the amount of available relevant field data becomes smaller. If only a few facts are known about the reservoir, a variety of theoretical reservoir models may explain these known facts equally well, but yield very different predictions of future potential. As the amount of field data available increases, of course, these uncertainties diminish. Thus, as time goes on, the understanding of the reservoir improves and forecasts become more reliable. Typically, the data base upon which numerical reservoir models are constructed consists of (1) geophysical surveys of various types, usually performed prior to development, (2) geological interpretations of underground structure, (3) downhole pressure and temperature surveys in shut-in wells, (4) flowing downhole surveys in wells, and (5) pressure-transient test results. Once exploitation begins in earnest, additional data become available, such as temporal trends in downhole flowing pressures and wellhead enthalpies. These latter data may be used in "history-matching" studies.

Since the uncertainty in the predictions of numerical reservoir models is directly related to the amount of field data available against which the models can be tested, the addition of repeat geophysical survey data to the above list of pertinent field measurements is likely to improve the reliability of the forecasts. It is well known in this connection that repeat precision gravity surveying has considerable promise for appraising the volumetric properties of any proposed mathematical reservoir model (e.g., Allis and Hunt, 1986; SanAndres and Pedersen, 1993; Ishido et al., 1995).

The application of improved geophysical techniques to reservoir management was among the objectives of a geothermal R&D project which was carried out by NEDO (the New Energy and Industrial Technology Development Organization) as a part of METI's New Sunshine Program from 1997 through 2002 (e.g., Horikoshi et al., 2001; Nakanishi et al., 2000; Pritchett et al., 2000; Ishido and Pritchett, 2000). GSJ (the Geological Survey of Japan) carried out supporting basic research in cooperation with NEDO, pursuing the development of improved field survey techniques and associated modeling studies involving geophysical survey techniques such as repeat gravity, self-potential, resistivity and seismic velocity surveys. In 2002, GSJ started a four-year cooperative research program, *"System Integration of Various Geophysical Measurements for Reservoir Monitoring"*, focused on the Okuaizu and Ogiri areas in Japan, to make practical applications of the results of the NEDO/GSJ project (e.g. Ishido et al., 2003; Ishido et al., 2005; Nishi et al., 2005; Sugihara et al., 2006; Sugihara and Ishido, 2008).

In the present paper, we will introduce recent improvements made in the self-potential, seismic and surface-deformation postprocessors, and present the results of history-matching studies based upon self-potential data taken at the Okuaizu field.

2. DEVELOPMENT OF GEOPHYSICAL POSTPROCESSORS

The so-called "geophysical postprocessors" are computational tools used to calculate temporal changes in geophysical observables that result from changing underground conditions computed by reservoir simulations. The purpose of the development is to enable us to use monitoring data from repeat and/or continuous geophysical measurements in history-matching studies (Figure 1). We first developed a microgravity postprocessor and subsequently a self-potential postprocessor under GSJ's geothermal programs (e.g. Pritchett, 1995; Ishido et al., 1995; Ishido and Pritchett, 1996; Ishido and Pritchett, 1999). Afterwards, postprocessors to calculate changes in subsurface electrical resistivity (DC or MT) and seismic observables were developed (Nakanishi et al., 2000; Pritchett et al. 2000; Stevens et al., 2000), and the existing gravity and SP postprocessors were also enhanced under the NEDO's project from 1997 to 2002. The application of various electrical postprocessors to field data was discussed by Garg et al. (2007). The postprocessors were originally developed for use with the "STAR" code (Pritchett, 1995). The reservoir simulation results required for postprocessor calculations are stored on STAR's "*GEO*" output file. If an interface program is developed to create an equivalent "*GEO*" file from reservoir simulation results, the postprocessors can be applied to the results obtained using other reservoir

simulators. Among relatively new developments, new capabilities and/or improvements added to the self-potential, seismic and surface-deformation postprocessors are described hereafter.

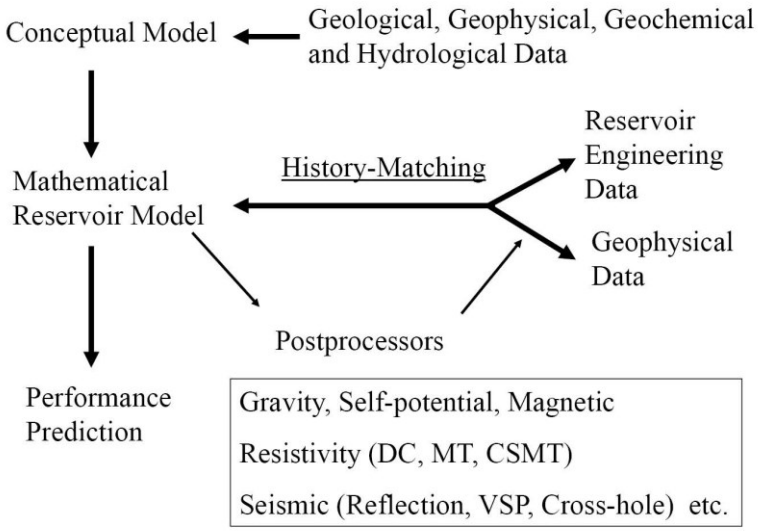

Figure 1: Geothermal reservoir modeling. Various computational postprocessors permit the user to calculate temporal changes that are likely to be observed if geophysical surveys of an operating geothermal field are repeated from time to time. Results may be used to supplement conventional reservoir engineering measurements in history-matching studies undertaken during geothermal reservoir model development.

2.1 Self-Potential Postprocessor

The self-potential postprocessor calculates changes in subsurface electrical potential induced by pressure disturbances through electrokinetic coupling (Ishido and Pritchett, 1999), so it is also called an "EKP-postprocessor". The postprocessor has been extensively applied to volcano SP studies (e.g. Ishido et al., 1997; Ishido, 2004; Aizawa et al., 2008; Onizawa et al., 2009) in addition to geothermal reservoir modeling. We have extended it to calculate electrokinetic potentials in fractured reservoirs that are represented as "MINC" double porosity media (Ishido and Pritchett, 2003), and applied it to fractured reservoir modeling (e.g. Ishido et al., 2003) and characterization (e.g. Nishi and Ishido, 2012a). Its "magnetic" variant was also developed to calculate changes in geomagnetic field due to electrokinetic coupling (by applying the Biot-Savart law to the distributions of drag and conduction current density) and due to temperature-dependent rock magnetization (Ishido and Pritchett, 2001).

In addition to electrokinetic coupling, SP anomalies may be generated by various other mechanisms such as thermoelectric coupling, electrochemical diffusion potential (Ishido and Pritchett, 2011), etc. In particular, SP anomalies of negative polarity, which are frequently observed near wells, appear to be caused by an underground electrochemical mechanism similar to a galvanic cell known as a "geobattery" (e.g. Bigalke and Grabner, 1997): the metallic well casing acts as a vertical electronic conductor connecting regions of differing redox potential. Electrons flow upward though the casing from a deeper reducing environment to a shallower oxidizing environment, and simultaneously a compensating vertical flow of ions is induced in the surrounding formation to maintain charge neutrality. If the redox potential in the deeper region is then increased by injecting an oxidizing substance, the difference in redox potential between the shallower and deeper regions will be reduced, resulting in an SP increase near the wellhead. Ishido et al. (2013) reported the results of numerical simulations carried out using the extended SP postprocessor (which incorporates the above geobattery mechanism in addition to electrokinetic coupling) and discussed the above possibility quantitatively.

2.2 Seismic Postprocessor

The seismic postprocessor is designed to predict temporal changes in seismic properties and the resulting changes in seismic observables such as travel time, attenuation and reflections that are caused by subsurface changes in the geothermal reservoir. In the original postprocessor (Stevens et al., 2003), the changes in seismic properties are predicted using Biot theory and empirical relationships. Changes to observables are then predicted by calculating the propagation of seismic waves through this structure. Since the geothermal simulation is in general performed on a coarse grid relative to the resolution required for seismic simulations, an interpolation scheme is developed to optimize prediction of observables and avoid artifacts induced by the coarseness of the geothermal grid. The seismic postprocessor can be used to predict the results of passive seismic surveys, reflection surveys, VSP surveys, and crosshole tomography surveys.

In order to apply the postprocessor to CCS (e.g. Ishido et al., 2011; Sugihara et al., 2013), we have developed a "patchy saturation" model (e.g. Mavko et al., 2009) to calculate P-wave velocity and Q factor in liquid/gas two phase zones. In this new model, the

low-frequency and high-frequency limiting bulk moduli are given by Gassmann's relation and by Hill's relation, respectively. The "standard linear solid" is applied to predict the velocity dispersion and attenuation with the characteristic frequency, which is inversely proportional to the square of liquid cluster size which depends on the liquid-phase saturation. Figure 2 shows seismic sections calculated by applying the new seismic (reflection survey) postprocessor to the reservoir simulation results. The reflected waves correspond to the upper and lower boundaries of regions containing CO_2 gas around the injection wells.

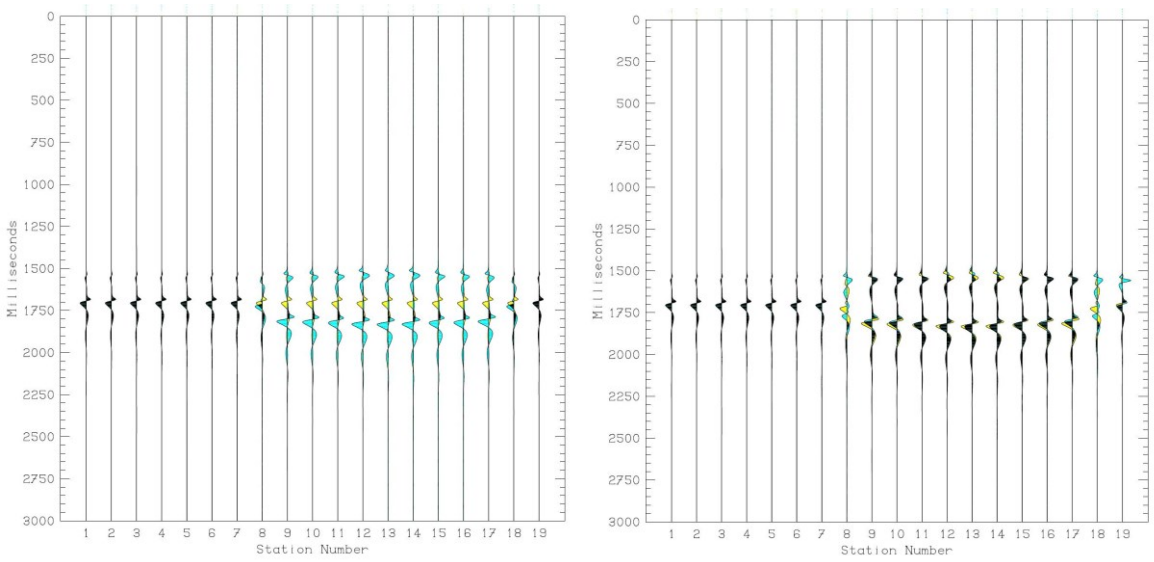

Figure 2: Comparison of time series between; (left) the surveys before CO_2 injection (yellow) and after 10-year CO_2 injection (blue), and (right) the surveys after 10-year CO_2 injection (yellow) and after 10-year shut-in. Overlapped traces for the two surveys are shown in black.

2.3 Surface-Deformation Postprocessor

The first version of the surface-deformation postprocessor was developed in 2000. The postprocessor calculates the surface deformation resulting from changes in reservoir pressure, temperature and mass distributions by using the "SUBSIDE" finite element geomechanical code (Sweet, 1999). Its improvement is presently in progress for its applications to CCS problems. Figure 3 shows comparisons of the computed results with an analytic solution given by the "Mogi" model.

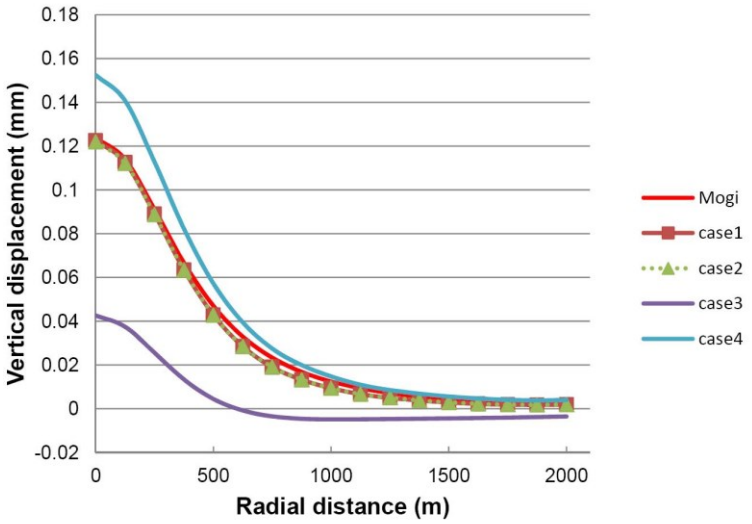

Figure 3: "Mogi" theoretical curve is for a spherical pressure source (radius=23.9 m, Δp=50 bars) located at 525 m depth. "Case 1" is calculated for a 50 m-size cubical pressure source, and "Case 2" is for an equivalent temperature source. "Case 3" and "Case 4" are for the pressure source, but the pore fluid (initial density=ρ_0) is replaced with denser (2.6 times ρ_0) and lighter (0.40 times ρ_0) fluid at the same time for "Case 3" and "Case 4", respectively.

3. HISTORY-MATCHING STUDY USING SP AND GRAVITY DATA

3.1 Repeated and Continuous SP Measurements at the Okuaizu Geothermal Field

The Okuaizu geothermal field is located in northeastern Japan and is characterized by northwest–southeast-trending vertical faults. Exploratory drilling surveys delineated a high-temperature reservoir along these faults, and the 65-MW generating capacity Yanaizu-Nishiyama geothermal power station started operation in May 1995. Most wells penetrating the Chinoikezawa and Sarukurazawa faults have been producing vapor-dominated excess enthalpy fluid, which suggests the growth of a liquid/vapor two-phase zone within the reservoir. All separated water and excess steam condensate are reinjected into a cooler zone around the Oisawa fault, which also trends northwest–southeast and is located in the northeast part of the field (e.g., Saeki, 1999).

In 1982-1983, the SP distribution in the natural state before fluid production was measured over this area as a part of the Geothermal Development Promotion Survey by NEDO (e.g. Nitta et al., 1987). A dominant SP anomaly of positive polarity over the high-temperature zone was detected from this survey (Figure 3). After the start-up of fluid production, GSJ carried out repeat SP surveys in November 1996 and May-September 1998 along a profile line across this anomaly area (Tosha et al., 2000). The positive SP anomaly over the high-temperature zone in the natural state was found to disappear in 1996, after ~18 months of fluid production (Figure 4). In 1998 fluid production was suspended for a short time (about two months) due to field wide shut-in for power station maintenance. A small positive anomaly appeared during the shut-in period (May 1998), and disappeared again after the re-start of fluid production (Tosha et al., 2000).

The observed SP changes are thought to be associated with substantial production-induced expansion of the vapor-dominated zone (due to reservoir pressure decline). Just below the vapor zone, vigorous boiling occurs and counterflows of vapor (upward) and liquid (downward) are produced. This downward flow of the liquid phase carries drag current with it and brings about a negative SP change at the ground surface (see e.g. Ishido and Pritchett, 1999).

In the next section, we will describe the results of preliminary history-matching studies by Nishi and Ishido (2012b), which show that the above-described process explains the SP changes observed by repeat surveys (mentioned above) and by continuous SP measurements during short term field-wide shut-ins in 2000, 2002 and 2004 (Nishi and Ishido, 2012b).

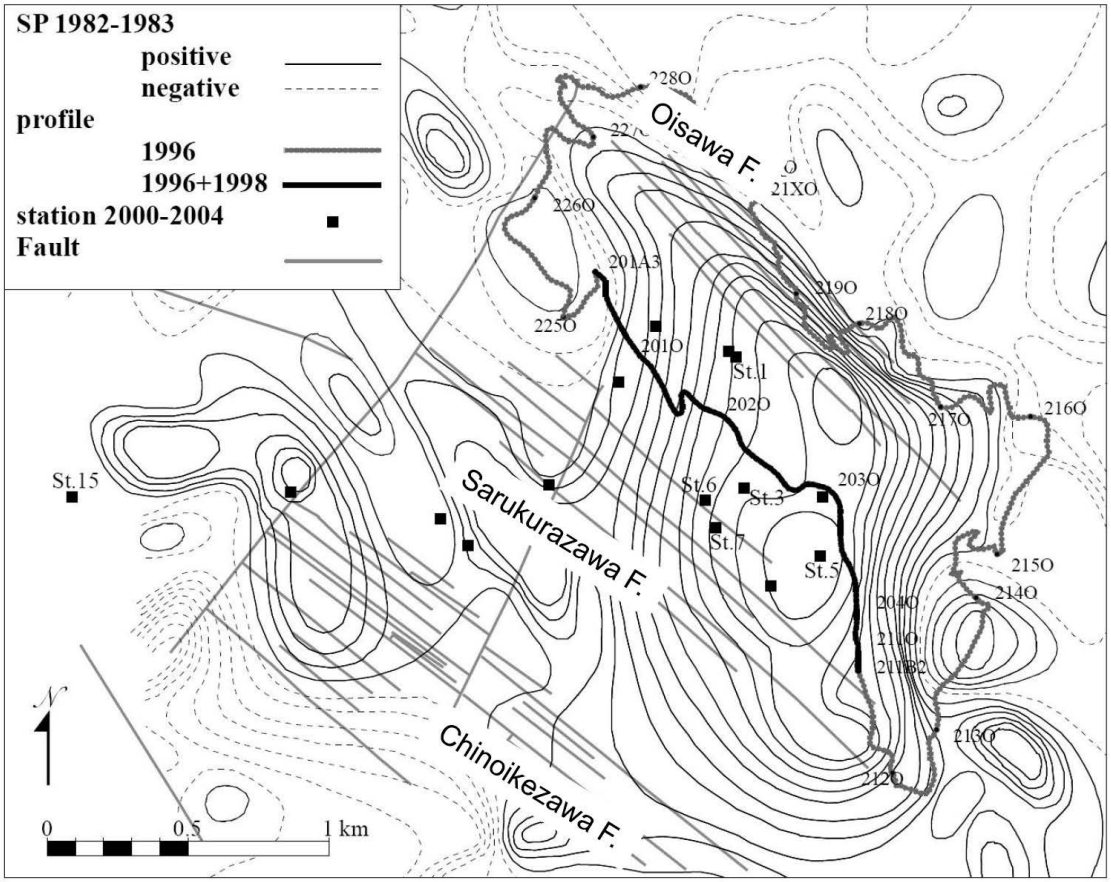

Figure 3: Self-potential (SP) distribution in the natural state. SP surveys in 1982-1983 revealed positive SP anomalies (solid contours) overlying three NW-SE trending faults (after Nitta et al., 1987). The locations of profile line for SP surveys in 1996 and 1998 (Tosha et al., 2000) and SP stations for continuous measurements from 2000 to 2004 (Nishi and Ishido, 2012) are also shown.

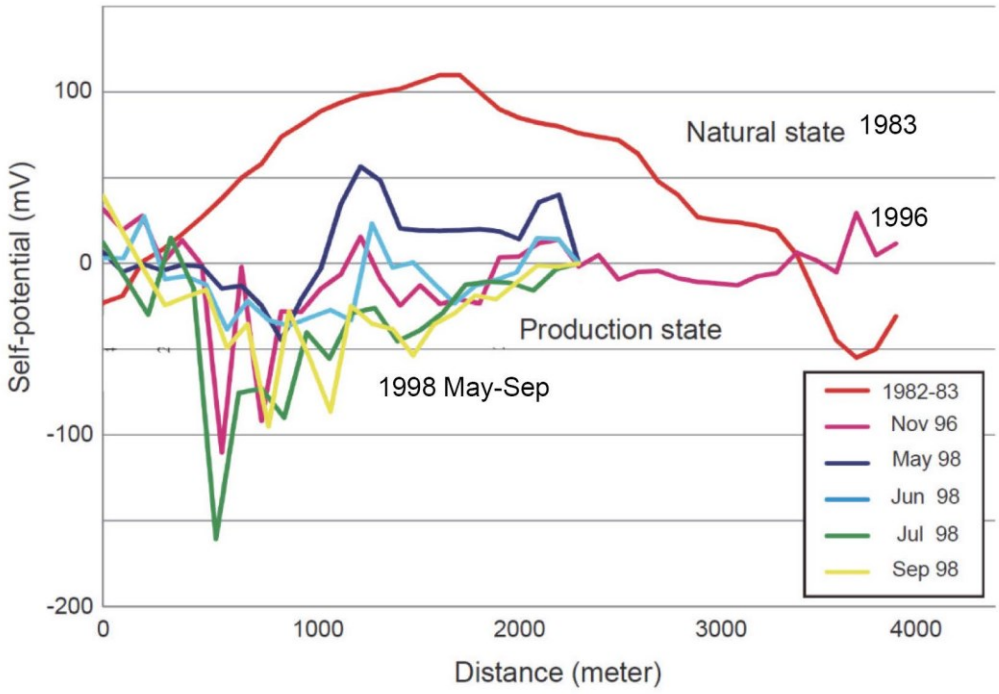

Figure 4: SP profiles along a survey line passing through the central part of the Okuaizu field. The red line shows the SP profile in the natural state, measured in 1982-83. The survey in November 1996 was carried out about 18 months after start-up of the Yanaizu-Nishiyama power station. The repeated surveys in 1998 were carried out after 2 months shut-in of production wells in April and May 1998 (after Tosha et al., 2000). The location of the profile line is shown in Figure 3.

3.2 Reservoir Model

Nishi and Ishido (2012b) tried to incorporate the observations mentioned in the previous section into a simple numerical reservoir model. This amounts to a history-matching study, but the reservoir structure was not built to reproduce actual production zones along the two nearly-vertical faults. Although the model roughly reproduces the power generation history for the first several years, locations and flow rates of production wells, etc., were not adjusted to reproduce the actual production wells and operation history.

A three-dimensional grid was used; it extends from x = 0 km to +3 km (along the NW-SE direction), y = -1.1 km to y = 1.1 km and z = -3 km RSL to 0 km RSL as shown in Figure 5. The computational grid consists of 3600 blocks (30 × 5 × 24). Seven rock formations are present, which differ in porosity and permeability (Table 1). Other formation properties are uniform: rock grain density is 2600 kg/m^3, rock heat capacity is 1 kJ/kg-°C, and thermal conductivity is 2 W/m-°C. Relative permeabilities are simple straight-line functions with residual water and steam saturations of 30% and 5% respectively. The high-permeability reservoir, which is subdivided into upper, main and deep reservoirs (both the main and deep reservoirs are of the "Reservoir" rock type in Table 1), is sandwiched by the low-permeability wall rocks and overlain by caprock.

Pressure and temperature are maintained at 30 - 40 bars and 80°C respectively along the top boundary at z = 0 km RSL (which corresponds to 0.5 km depth). All vertical boundaries except a part of the surface at x = 0 km are impermeable and insulated; pressure is maintained at 14.8 MPa in the "recharge" block located at x = 0, y = 0 and z = -1.4 km RSL so as to allow outflow or inflow at the vertical boundary. Most of the bottom surface (at z = -3 km RSL) is impermeable, but constant temperature (280 - 330°C) is imposed over the bottom surface at 1.5 km < x < 3 km and -0.2 km < y < 0.2 km. A source of high-temperature water (330 ºC, containing mass fractions of 0.06 of CO_2 and 0.003 of NaCl) was imposed along a portion of the bottom surface (1.5 km < x < 3 km and -0.1 km < y < +0.1 km) with a total inflow rate of 8.4 kg/s.

After a few tens repetition of parameter adjustments and natural-state and exploitation simulations, Nishi and Ishido reached a final model. Here we consider their final *"MINC1"* model and three variants of the final model: *"MINC2"*, *"MINC3"* and *"POROUS"*. Although all of these models have the same common features described above, the formations representing the upper, main and deep reservoirs are assumed to be "MINC" double-porosity media for the *"MINC1"*, *"MINC2"* and *"MINC3"* models and to be equivalent porous media for the *"POROUS"* model (Table 1).

The development of the "natural state" hydrothermal convection system was computed for the *"POROUS"* model using the STAR geothermal reservoir simulator (Pritchett, 1995; Pritchett, 2002). The system reached quasi-steady state after around 100,000 years of evolution. Although a two-phase steam/water zone develops at shallow levels of the reservoir below the caprock, most of the reservoir is under hydrostatic conditions as observed for the Okuaizu reservoir before the start-up of the power station (see upper left image of Figure 7).

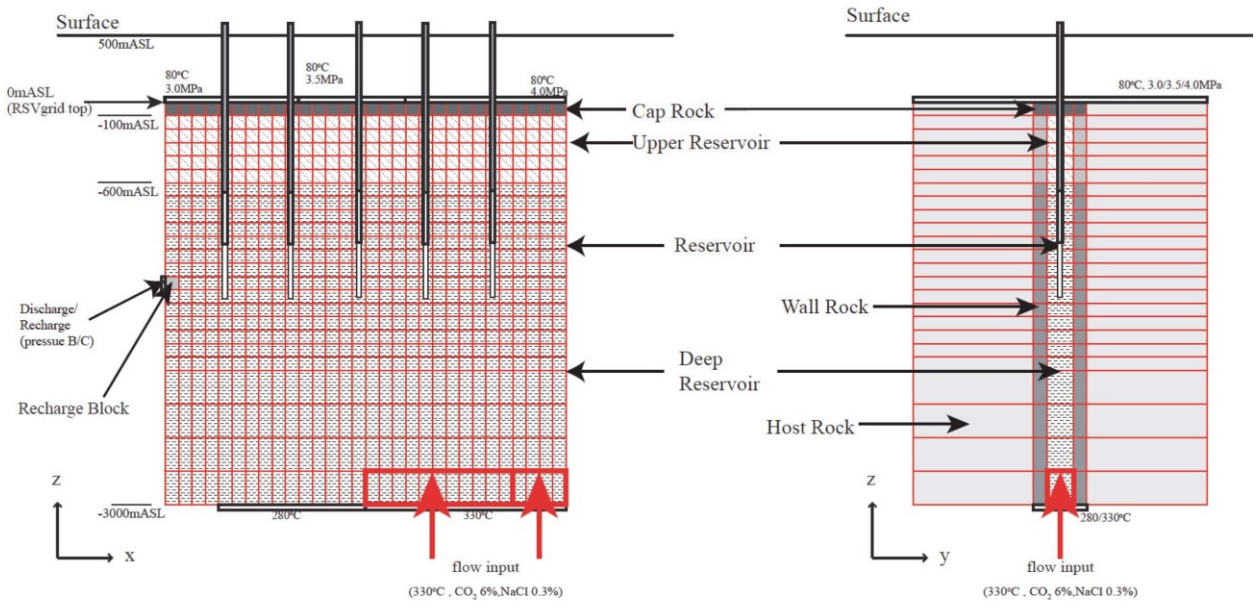

Figure 5: Numerical model used for reservoir simulation. The reservoir in the Okuaizu field is simplified as a vertical moderate-permeability reservoir, surrounded by very-low permeability caprock and wall rock regions. See Table 1 for details of rock properties. Boundary conditions and location of production wells (which are hypothetical in locations, etc.) are also shown. In the SP-postprocessor calculations low resistivity zones are assumed between the earth's surface (at 500 mRSL) and the top of simulation grid (at 0 mRSL) based upon the near surface resistivity structure at the Okuaizu field.

Table 1 Rock types and pertinent parameters used in numerical simulations.

Rock Type	Model	Cap Rock	Upper Reservoir	Reservoir	Upper Wall Rock	Wall Rock	Host Rock	Host Rock
Medium	Porous	Porous	Porous -18	Porous -20	Porous	Porous	Porous	Porous
	MINC1		MINC-18	MINC-20				
	MINC2		MINC-18	MINC-18				
	MINC3		MINC-20	MINC-20				
Porosity		0.05	0.1	0.1	0.05	0.05	0.1	0.1
Permeability $\times 10^{-15}$ (m^2)	k_x	1.0E-03	50	10	0.1	1.0E-5	1	0.5
	k_y	1.0E-03	50	10	0.1	1.0E-5	1	0.5
	k_z	1.0E-03	5	10	0.1	1.0E-5	1	0.5

Medium	MINC-20	MINC-18
fracture volume fraction	0.05	0.05
fracture spacing (m)	30	30
matrix permeability $\times 10^{-15}$ (m^2)	1.0E-5	1.0E-3

3.3 Exploitation Calculation

The STAR simulator was next used to perform a 10-year forecast of the consequences of production, starting from the natural-states calculated for the *"POROUS"* model as the initial conditions. All boundary conditions and rock properties other than for "Upper Reservoir" and "Reservoir" are the same as those used to calculate the natural-state. The calculations were carried out by using STAR's capability to treat "geothermal power systems", which allows us to allocate fluid production rate to various wells so as to maintain a given power generation scenario. Initially ten production wells are active; five wells have shallow feed-points at z = -650 m RSL and the other five wells have intermediate-depth feed-points at z = -1050 m RSL to maintain 60 MW for the first two years and 40 MW for the subsequent eight years (30-day shut-in is assumed every 360 days). In the calculation five deep makeup

wells are provided for, the feed-points of which are located at z = -1450 m RSL. All fifteen production wells are hypothetical and their feed-points are located in the "Reservoir" formation. No reinjection of waste fluid takes place in these calculations: in the actual Okuaizu field, reinjection takes place in a cooler zone around the Oisawa fault which is hydraulically disconnected from the production zones around the Chinoikezawa and Sarukurazawa faults (e.g. Saeki et al., 1999).

Figure 6 shows 10-year histories of computed power generation and produced fluid enthalpy. Although full power generation is not maintained for the entire ten years using the *"MINC1"* and *"MINC3"* models, the produced fluid enthalpy increases rapidly during the first year in these cases. This so-called "excess enthalpy effect" is caused by a very low matrix region permeability ($k_m = 10^{-20}$ m^2) for the "MINC-20" medium, which is assumed for the "Reservoir" formation in both cases. When production-induced boiling begins in the fracture zones, decline in pressure and temperature induces mass and heat transfer from the matrix region to the fracture zones. However, so long as the matrix region permeability is significantly less than one microdarcy under two-phase conditions, it is possible to neglect the mass transfer from matrix to fractures, and treat heat transfer as arising from unsteady heat conduction only (e.g. Pritchett, 2005). The rapid increase in produced fluid enthalpy actually observed at the Yanaizu –Nishiyama power station can be best explained by the *"MINC1"* or *"MINC3"* model among the four models considered here.

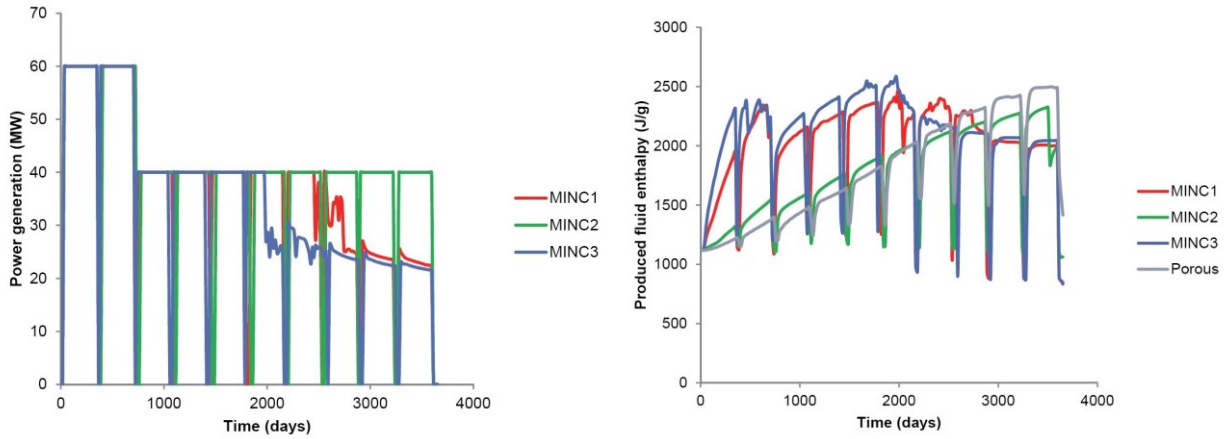

Figure 6: Histories of power generation (left) and produced fluid enthalpy (right). To maintain "desired output", the "STAR" reservoir simulator assigns flow-rate to each production well with 0.63 MPa wellhead pressure. The desired output cannot be maintained due to decline of some of the available production wells after 5 years and 7 years in the *"MINC3"* and *"MINC1"* cases respectively, although these two models reproduce the rapid increase in produced fluid enthalpy during the first few years of plant operation quite well.

3.4 Changes in Self-Potential and Gravity

Next, STAR's self-potential postprocessor (see, e.g. Ishido and Pritchett, 1999; Ishido and Pritchett, 2003) was used to calculate the self-potential changes at the earth surface which are caused by changes in underground conditions that result from production.

3.4.1 Outline of Self-Potential Postprocessor

The self-potential postprocessor calculates space/time distributions of electrokinetic potentials resulting from histories of underground conditions (pressure, temperature, salt concentration, liquid-phase saturation, etc.) computed by reservoir simulations (as mentioned in section 2.1). The basic equation solved by the postprocessor is:

$$-\nabla \cdot \mathbf{I}_{\mathrm{cond}} = \nabla \cdot \mathbf{I}_{\mathrm{drag}} \tag{1}$$

where $\mathbf{I}_{\mathrm{cond}}$ (= $-L_{ee}\nabla\phi$) is a conduction current density caused by the electric potential gradient ($\nabla\phi$), and $\mathbf{I}_{\mathrm{drag}}$ (= $-L_{ev}\nabla\xi$) is a drag current density caused by charges moved by fluid flow (due to the driving force $\nabla\xi = \nabla p + \rho\mathbf{g}$) through electrokinetic coupling (here, L_{ee}: electrical conductivity of fluid/rock composite, and L_{ev}: cross-coupling coefficient).

Based upon a capillary model, the above coefficients L_{ee} and L_{ev} may be written as follows (e.g. Ishido and Mizutani, 1981):

$$L_{\mathrm{ee}} = F^{-1}\left(\sigma + m^{-1}\Sigma_S\right) \tag{2}$$

$$L_{\mathrm{ev}} = -F^{-1}\varepsilon\zeta R_{ev} G/\mu \tag{3}$$

where F = electrical formation factor (F^{-1} = [porosity]/[square of tortuosity]), σ = electrical conductivity of pore fluid, m = hydraulic radius of pores and/or cracks, which equals half of radius and aperture for pores with circular and slit-like cross-sections, respectively, Σ_s = surface conductance, ε = liquid-phase dielectric permittivity, ζ = zeta-potential, R_{ev} = "electrical relative

permeability" for two-phase flow, G = a correction factor which becomes less than unity only if the hydraulic radius is comparable to the thickness of the electrical double layer (Ishido and Pritchett, 1999), and μ = liquid-phase viscosity.

The self-potential postprocessor simulates electric potentials caused by subsurface fluid flow by a two-step process. First, it calculates the distribution of L_{ev}, L_{ee} and $\mathbf{I}_{\mathrm{drag}}$ from the reservoir-simulation results using the same spatial grid used for the reservoir simulation calculation. Next, the postprocessor calculates the electric potential (ϕ) distribution by solving the above Poisson equation (1) within a finite-difference grid that is usually much greater in spatial extent than the grid used for reservoir simulation.

Ishido and Pritchett (2003) extended the self-potential postprocessor so as to calculate the drag current density in "MINC" media (as mentioned in section 2.1). In the MINC representation, the contribution of mass exchange through the matrix region is neglected in mass exchange between adjacent macroscopic computational grid blocks. However, the contribution through the matrix region is not negligible for the drag current density. This is because the magnitude of the drag current is not proportional to the permeability, but to F^{-1}. The contribution of the matrix region is small at early times, but usually predominates under steady-state conditions.

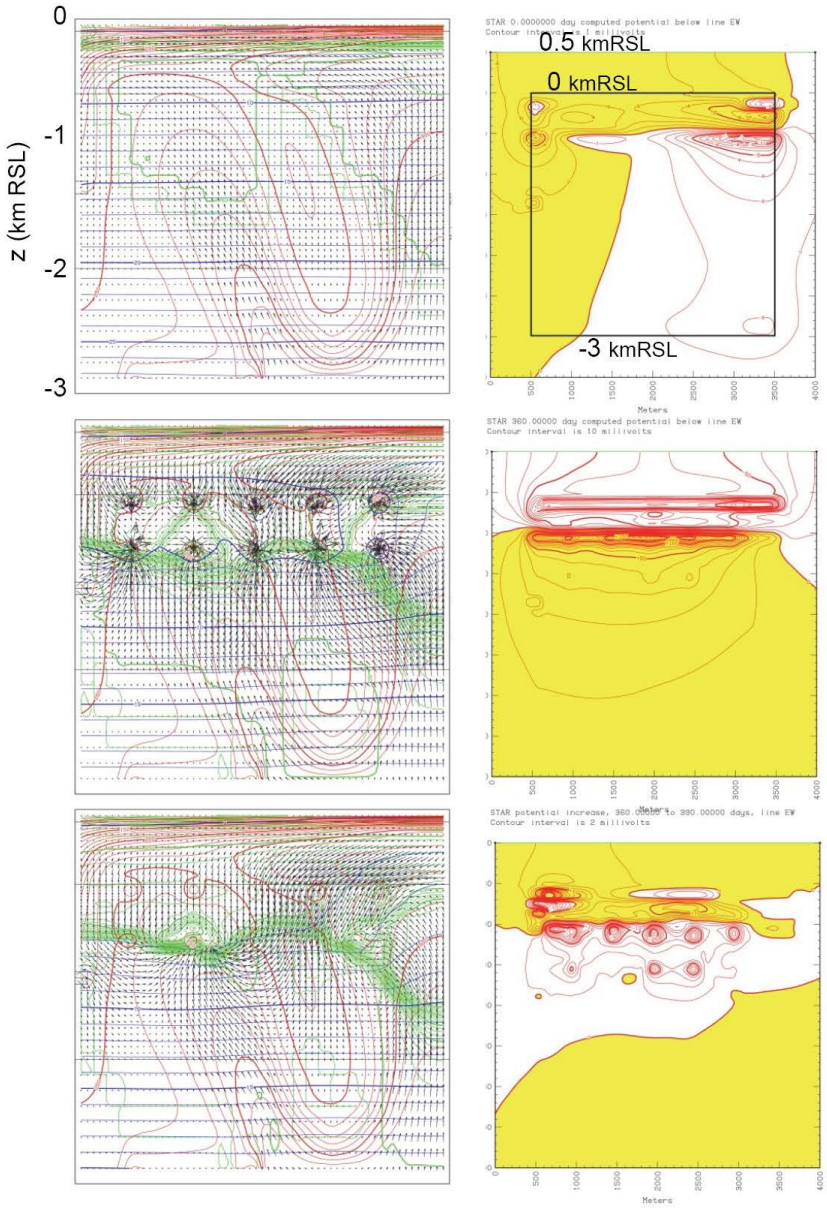

Figure 7: Vertical section of reservoir conditions: pressure, temperature, liquid-phase saturation and mass flow-rate (left) and self-potential distributions (right) calculated for the *"MINC1"* model. The results are shown for the natural state (upper), after 1 year of fluid production (middle), and after 30 days field-wide shut-in at 1 year (lower). In the left figures, contour interval is 1 MPa for pressure (in blue), 10 °C for temperature (in red), and 0.05 for liquid-phase saturation (in green). In the right figures, snapshots of SP distribution (upper) and (middle), and SP change during the 30-day shut-in (lower) are shown. Yellow colored area indicates positive SP region, and contour interval is 1 mV, 10 mV and 2 mV, respectively, for (upper), (middle) and (lower) plots.

3.4.2 Postprocessor Calculations

Among the various parameters in equations (2) and (3), F^{-1} and m^{-1} (or $m^{-1}\Sigma_S$) are input parameters and assigned for each rock formation; in case of a MINC medium, these are assigned separately for the fracture and matrix regions. G in (3) is assumed to be unity for all formations except for the matrix region of the "MINC-20" medium, for which a very small G (<< 1) is assumed. This assumption is plausible since the hydraulic radius is less than the electrical double layer thickness for low permeability ($k_m = 10^{-20}$ m^2) intact rocks (e.g. Ishido and Matsushima, 2007). When setting parameter values, we also tried to reproduce the resistivity structure revealed by MT surveys at the Okuaizu field (Takakura, 2003).

Figure 7 (upper) and (middle) show the distributions of SP under natural state conditions and after one year of fluid production, respectively, with the corresponding reservoir conditions. As seen in the figure, exploitation drastically changes the SP distribution; downward liquid flow in the production-induced boiling zone causes corresponding drag currents, resulting in negative potentials at shallower levels. Although a large subsurface positive potential appears associated with the production zone, it is confined to the immediate neighborhood of the production well feed-points. As shown in the lower plots, SP in shallow regions recovers by a few millivolts during the 30-day field-wide shut-in, which corresponds to decrease in the rate of downward liquid flow.

Figure 8 (left) shows temporal changes in self-potential at a station located in the central production area. SP rapidly decreases more than 50 mV during the first few years of fluid production for the *"MINC1"*, *"MINC2"* and *"POROUS"* models. In a MINC medium, the contribution from drag currents in the matrix region is important due to its significant volume fraction (0.95). However, in case of the *"MINC3"* model, change in SP is very small compared to other cases. This is because all of reservoir regions including the "Upper Reservoir" consist of the "MINC-20" medium, in which the drag current in the matrix region is negligibly small due to very small assigned value of G as described above.

Figure 8 (right) shows temporal changes in gravity calculated using the gravity postprocessor. Among the three MINC models, the gravity decrease is smallest for *"MINC3"* and largest for *"MINC2"*. These results reflect changes in liquid-phase saturation in the matrix region, which remains high after 10 years in the reservoir region represented by the "MINC-20" medium. The calculated gravity changes for the *"MINC1"* and *"MINC2"* models are in the range of long-wavelength micro-gravity decline actually observed between 1997 and 2000 (NEDO, 2003).

As shown in Figure 8 (left), short-term SP changes appear associated with 30-day shut-ins every 360 days only in the *"MINC1"* and *"MINC2"* results. These short-term changes are caused by the above-mentioned mechanism. Although we need a three-dimensional model which reproduces the actual reservoir conditions in more detail to discuss such short-term and relatively small magnitude signals, SP increases of 5-10 mV detected by continuous SP measurements during short term field-wide shut-ins in 2000, 2002 and 2004 (Nishi and Ishido, 2012b) are fairly well reproduced by the *"MINC1"* result.

In summary, the rapid increase in produced fluid enthalpy during the first few years of fluid production can be reproduced by the *"MINC1"* or *"MINC3"* model, in which the "Reservoir" is represented by the "MINC-20" medium (matrix region permeability k_m is low enough not to allow mass transfer to fracture zones). However, changes in SP and gravity cannot be explained by the *"MINC3"* model, in which the "Upper Reservoir" is represented by the "MINC-20" medium, but can be explained by the *"MINC1"* model, in which the "Upper Reservoir" is represented by the "MINC-18" medium (k_m is high enough to allow mass transfer to fracture zones and substantial electrokinetic coupling). The short-term SP changes associated with field-wide shut-ins provide additional evidence supporting the *"MINC1"* model. Reflecting the difference in k_m in the "Upper Reservoir" between the *"MINC3"* and *"MINC1"* models, the desired project electrical output (shown in Figure 6) is maintained two years longer for *"MINC1"* than for *"MINC3"*.

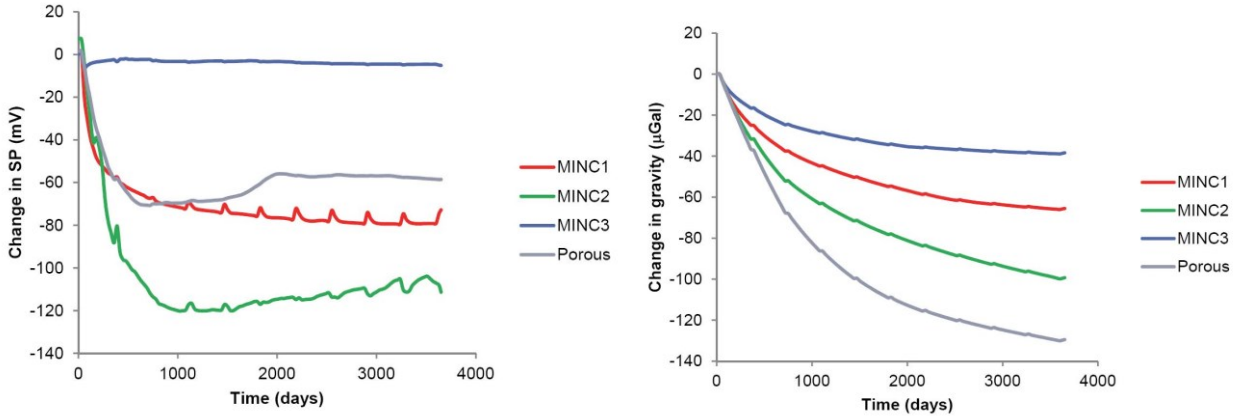

Figure 8: Temporal variations of SP and gravity at "CENTER" station. Short-term SP changes associated with shut-ins every 360 days appear only in the results of *"MINC1"* and *"MINC2"* models.

4. CONCLUDING REMARKS

The use of surface geophysical survey methods to monitor subsurface changes in geothermal reservoirs arising from production and injection operations is attracting increasing attention as an approach to better understand subsurface changes and to provide additional constraints for history-matching studies used to calibrate proposed predictive reservoir models. Computational postprocessors have been developed to permit the forward calculation of observable changes in time-lapse surveys such as microgravity, self-potential, DC resistivity, MT, seismic, etc. based on the results of traditional reservoir simulation calculations. In order to provide better constraints on history-matching studies, further improvements of the postprocessors are in progress particularly for various constitutive laws used to calculate geophysical observables from reservoir conditions.

REFERENCES

Aizawa, K., Ogawa, Y., and Ishido, T.: Groundwater Flow and Hydrothermal Systems Within Volcanic Edifices: Delineation by Electric Self-Potential and Magnetotellurics, *J. Geophys. Res.*, **114**, Article ID B01208, (2009).

Allis, R.G., and Hunt, T.: Analysis of Exploitation-Induced Gravity Change at Wairakei Geothermal Field, *Geophysics*, **51**, (1986), 1647-1660.

Bigalke J, and Grabner, E.W.: The Geobattery Model: a Contribution to Large Scale Electrochemistry, *Electrochimica Acta*, **42**, (1997), 3443-3452.

Garg, S.K., Pritchett, J.W., Wannamaker, P.E., and Combs, J.: Characterization of Geothermal Reservoirs with Electrical Surveys: Beowawe Geothermal Field, *Geothermics*, **36**, (2007), 487–517.

Horikoshi, T., Yamasawa, S., Ide, T., and Tosha, T.: NEDO's Project on Development of Technology for Reservoir Mass and Heat Flow Characterization (1) Project Outline and Techniques to Improve the Reservoir Model, *GRC Transactions*, **25**, (2001), 641–644.

Ishido, T., and Muzutani, H.: Experimental and Theoretical Basis of Electrokinetic Phenomena in Rock-Water Systems and Its Applications to Geophysics, *J. Geophys. Res.*, **86**,(1981), 1763-1775.

Ishido, T., Sugihara, M, Pritchett, J.W., and Ariki, K.: Feasibility Study of Reservoir Monitoring Using Repeat Precision Gravity Measurements at the Sumikawa Geothermal Field, *Proceedings,* World Geothermal Congress, Florence (1995).

Ishido, T. and Pritchett, J.W.: Numerical Simulation of Electrokinetic Potentials Associated with Subsurface Fluid Flow, *Proceedings,* 21st Workshop on Geothermal Reservoir Engineering, Stanford University, Stanford, CA (1996).

Ishido, T., Kikuchi, T., Matsushima, N., Yano, Y., Nakao, S., Sugihara, M., Tosha, T., Takakura, S., and Ogawa, Y.: Repeated Self-Potential Profiling of Izu-Oshima Volcano, Japan, *J. Geomag. Geoelec.*, **49**, (1997), 1267-1278.

Ishido, T., and Pritchett, J.W.: Numerical Simulation of Electrokinetic Potentials Associated with Subsurface Fluid Flow, *J. Geophys. Res.*, **104**, (1999), 15247-15259.

Ishido, T., and Pritchett, J.W.: Using Numerical Simulation of Electrokinetic Potentials in Geothermal Resource Management, *Proceedings*, World Geothermal Congress, Beppu-Morioka (2000).

Ishido, T., and Pritchett, J.W.: Prediction of Magnetic Field Changes Induced by Geothermal Fluid Production and Reinjection, *GRC Transactions,* **25**, (2001).

Ishido, T., and Pritchett, J.W.: Characterization of Fractured Reservoirs Using Continuous Self-Potential Measurements *Proceedings,* 28th Workshop on Geothermal Reservoir Engineering, Stanford University, Stanford, CA (2003).

Ishido, T., Goko, K., Tosha, T., Adachi, M., Ishizaki, J., and Nishi, Y.: Reservoir Monitoring Using Multi-Geophysical Survey Techniques, *GRC Transactions*, **27**, (2003), 827-831.

Ishido, T.: Electrokinetic Mechanisms for the "W"-Shaped Self-Potential Profile on Volcanoes, *Geophys. Res.Lett.*, **31**, Article ID L15616, (2004).

Ishido, T., Goko, K., Adachi, M., Ishizaki, J., Tosha, T., Nishi, Y., Sugihara, M., Takakura, S., and Kikuchi, T.: System Integration of Various Geophysical Measurements for Reservoir Monitoring, *Proceedings*, World Geothermal Congress, Antalya (2005).

Ishido, and Matsushima, N.: Streaming Potential Measured for an Intact Rock Sample at Temperatures to 200°C, *Proceedings*, 32nd Workshop on Geothermal Reservoir Engineering, Stanford University, Stanford, CA (2007).

Ishido, T., Tosha, T., Akasaka, C., Nishi, Y., Sugihara, M., Kano, Y., and Nakanishi, S.: Changes in Geophysical Observables Caused by CO_2 Injection into Saline Aquifers, *Energy Procedia*, **4**, (2011), 3276-3283.

Ishido, T., and Pritchett, J.W.: Effects of Diffusion Potential on Self-Potential Distribution in Geothermal Areas, *GRC Transactions*, **35**, (2011).

Ishido, T., Pritchett, J.W., Tosha, T., Nishi, Y., and Nakanishi, S.: Monitoring Underground Migration of Sequestered CO_2 Using Self-Potential Methods, *Energy Procedia*, **37**, (2013), 4077-4084.

Mavko, G, Mukerji, T., and Dvorkin, J.: The Rock Physics Handbook, 2nd ed. Cambridge Univ. Press (2009).

Nakanishi, S., Ariki, K., Pritchett, J.W., and Yamazawa, S.: Integrated Numerical Reservoir Modeling Coupled with Geophysical Monitoring Techniques, *Proceedings*, World Geothermal Congress, Beppu-Morioka (2000).

NEDO: Manual for "Technology for Reservoir Mass and Heat Flow Characterization", NEDO report, 479pp., (2003).

Nishi, Y., Ishido, T., Sugihara, M., Tosha, T., Adachi, M., Saeki, K., and Ishizaki, J.: Reservoir Monitoring in the Okuaizu Geothermal Field Using Multi-Geophysical Survey Techniques, *Proceedings*, World Geothermal Congress, Antalya (2005).

Nishi, Y., and Ishido, T.: Characterization of Fractured Reservoirs Using a Combination of Downhole Pressure and Self-Potential Transient Data, *Inter. J. Geophysics*, **2012**, Article ID 148919, doi:10.1155/2012/148919, (2012a).

Nishi, Y., and Ishido, T.: Self-potential Measurements for Reservoir Monitoring at the Okuaizu Geothermal Field, *J. Geother. Res. Soc. Japan*, **34**, (2012b), 71-90.

Nitta, T., Suga, S., Tsukagoshi, S., and Adachi, M.: Geothermal Resources in the Okuaizu, Tohoku District, Japan, *Chinetsu*, **24**, (1987), 340-370.

Onizawa, S., Matsushima, N., Ishido, T., Hase, H., Takakura, S., and Nishi, Y.: Self-Potential Distribution on Active Volcano Controlled by Three-Dimensional Resistivity Structure in Izu-Oshima, Japan, *Geophys. J. Inter.*, **178**, (2009), 1164-1181.

Pritchett, J.W.: STAR – a Geothermal Reservoir Simulation System, *Proceedings,* World Geothermal Congress, Florence (1995).

Pritchett, J.W., Stevens, J., Wannamaker, P., Nakanishi, S., and Yamazawa, S.: Theoretical Feasibility Studies of Reservoir Monitoring Using Geophysical Survey Techniques, *Proceedings,* World Geothermal Congress, Beppu-Morioka (2000).

Pritchett, J.W.: STAR User's Manual Version 9.0, SAIC-02/1055, (2002).

Pritchett, J.W.: Dry-Steam Wellhead Discharges from Liquid-Dominated Geothermal Reservoirs: a Result of Coupled Nonequilibrium Multiphase Fluid and Heat Flow Through Fractured Rock, *Geophysical Monograph Series*, **162**, AGU, (2005), 175-181.

Saeki, K.: History and the Present Status of the Yanaizu-Nishiyama Geothermal Project, *J. Geother. Res. Soc. Japan*, **21**, (1999), 237-247.

SanAndres, R.B., and Pedersen, J.R.: Monitoring the Bulalo Geothermal Reservoir, Philippines, Using Precision Gravity Data, *Geothermics*, **22**, (1993), 395–402.

Stevens, J.L., Pritchctt, J.W., Garg, S.K., Ariki, K., Nakanishi, S., and Yamazawa, S.: Seismic Methods for Observing Geothermal Field Evolution, *Proceedings,* World Geothermal Congress, Beppu-Morioka (2000).

Stevens, J.L., Pritchett, J.W., Garg, S.K., Ishido, T., and Tosha, T.: Prediction of Seismic Observables From Geothermal Reservoir Simulations. *GRC Transactions*, **27**, (2003), 841-846.

Sugihara, M., Ishido, T., and Horikoshi, T.: Short-Term Microgravity Changes Due to Shut-In of Production and Reinjection Wells, the Ogiri Geothermal Field, Japan, *GRC Transactions*, **30**, (2006), 965–970.

Sugihara, M., and Ishido, T.: Geothermal Reservoir Monitoring with a Combination of Absolute and Relative Gravimetry, *Geophysics*, **73**, (2008), WA37–WA47.

Sugihara, M., Nawa, K., Nishia, Y., Ishido, T., and Soma, N.: Continuous Gravity Monitoring for CO_2 Geo-Sequestration, *Energy Procedia*, **37**, (2013), 4302 – 4309.

Sweet, J.: SUBSIDE, a Finite Element Program for the Determination of Subsidence Resulting from Reservoir Production, Report CAI-099-100 Rev.2, (1999).

Takakura, S.: Resistivity Structure at the Okuaizu Geothermal Area Inferred from High-Density DC Resistivity and MT Surveys, *AIST report* AIST03-C00018, IR5-6, (2003).

Tosha, T., Ishido, T., Matsushima, N., and Nishi, Y.: Self-potential Variation at the Yanaizu-Nishiyama Geothermal Field and Its Interpretation by the Numerical Simulation, *Proceedings,* World Geothermal Congress, Beppu-Morioka (2000).